On the Equivalence of Two Schemes for Convective Momentum Transport

David M. Romps

Department of Earth and Planetary Science, University of California, Berkeley, and Earth Sciences Division, Lawrence Berkeley National Laboratory, Berkeley, California

ABSTRACT

The Gregory–Kershaw–Inness (GKI) parameterization of convective momentum transport, which has a tunable parameter C, is shown to be identical to a parameterization with no pressure gradient force and a mass flux smaller by a factor of $1 - C$. Using cloud-resolving simulations, the transilient matrix for momentum is diagnosed for deep convection in radiative–convective equilibrium. Using this transilient matrix, it is shown that the GKI scheme underestimates the compensating subsidence of momentum by a factor of $1 - C$, as predicted. This result is confirmed using a large-eddy simulation.

1. Introduction

As clouds convect, they transport horizontal momentum in the vertical. This process is referred to as convective momentum transport (CMT), and several schemes for parameterizing its effect have been proposed (e.g., Schneider and Lindzen 1976; Zhang and Cho 1991; Gregory et al. 1997, hereafter GKI) for use in general circulation models (GCMs). It has been shown that the choice of CMT scheme can have a significant impact on both the mean climate (Wu et al. 2007; Richter and Rasch 2008; Kim et al. 2008) and the interseasonal variability (Neale et al. 2008; Kim et al. 2008). This paper is motivated by this demonstrated impact of CMT on climate simulations and the uncertainty surrounding how to parameterize it.

It has been known for many years that organized convective systems, such as squall lines, can intensify existing shear by transporting momentum upgradient (Moncrieff and Miller 1976; LeMone 1983; Moncrieff 1992). These systems have been studied using both observations (e.g., Sanders and Emanuel 1977; Lin et al. 1986) and numerical simulations (e.g., Moncrieff and Miller 1976; Lafore et al. 1988). In contrast, unorganized convection tends to transport momentum downgradient (Lemone et al. 1984), but there is no consensus on how to parameterize this process. In this paper, we will study CMT in unorganized convection with the aid of a cloud-resolving model, which has proven to be a useful tool in the study of momentum transport (e.g., Soong and Tao 1984; Tao and Soong 1986; Mapes and Wu 2001; Robe and Emanuel 2001; Zhang and Wu 2003; Lane and Moncrieff 2010). The goal is to learn how best to parameterize CMT in general circulation models.

Clouds and the environment exchange horizontal momentum through two mechanisms. The first mechanism is the physical exchange of mass via convective entrainment and detrainment. In the bulk-plume equations, the horizontal force induced by this exchange is uniquely specified by the entrainment and detrainment rates. The second mechanism is the horizontal pressure force, which relaxes the cloud momentum and environmental momentum toward one another by equal and opposite measure. Here, we consider two schemes that differ in their treatment of the pressure gradient force.

The first approach represents the pressure force as some function of the difference in horizontal velocity between the cloud and the environment,

$$F = F(v - v_c),$$

where v and v_c are the environmental wind and cloud wind, respectively. We will refer to this type of parameterization as a drag-law (DL) scheme. Drag-law schemes have been used in the modeling of momentum transport for many decades (e.g., Malkus 1952; Newton and Newton 1959; Hitschfeld 1960; Newton 1966; Austin and Houze 1973; Houze 1973; Sui et al. 1989). Included within the

Corresponding author address: David M. Romps, Department of Earth and Planetary Science, University of California, Berkeley, 377 McCone Hall, Berkeley, CA 94720.
E-mail: romps@berkeley.edu

set of DL schemes is the zero-drag (ZD) approximation (Schneider and Lindzen 1976; Shapiro and Stevens 1980; Sui et al. 1989), defined as

$$F = 0,$$

which is a suitable approximation for sufficiently large updrafts (Newton and Newton 1959; Hitschfeld 1960).

The second approach, due to GKI, is to approximate the pressure force as proportional to the updraft velocity and the environmental shear, which gives

$$F = CM\partial_z v,$$

where C is a positive constant, M is the convective mass flux, and v is the environmental wind. This is the default scheme in the Community Atmosphere Model, version 5.1 (CAM5.1; Neale et al. 2010). Note that this representation of the pressure force has no dependence on v_c. This can lead to some unusual consequences: if a cloud is both rising and moving relative to the air in the direction of shear, then this force would accelerate the cloud rather than decelerate it.

The theoretical underpinnings for the GKI scheme are an analysis of linearized equations and a dominant-balance argument for the Poisson equation for pressure. In the analysis of linearized equations, the base state is an atmosphere with vertical shear but no vertical motion (Rotunno and Klemp 1982; Wu and Yanai 1994). Since the linearized equations cannot represent convective momentum transport (which would be quadratic in the deviations), it is not clear how relevant this analysis is to CMT. In the dominant-balance argument, several terms are discarded (including those responsible for all of the form drag in 2D and most of the form drag in 3D) to arrive at an approximate Poisson equation, defined as

$$-\nabla^2(p'/\rho) \approx 2\partial_z \mathbf{u}_h \cdot \nabla_h w,$$

where a subscript h denotes horizontal vector components. It is then assumed that $\partial_z \mathbf{u}_h$ is equal to the vertical shear in the environment, as motivated by the linear analysis (LeMone et al. 1988, p. 323). There is no consensus on the value of C, with GKI recommending $C = 0.7$, Zhang and Wu (2003) suggesting $C = 0.55$, and CAM using $C = 0.4$ (Neale et al. 2010). With in situ observations of the pressure field around storms (e.g., Ramond 1978; LeMone et al. 1988; Jorgensen et al. 1991), it is difficult to differentiate between competing theories in the absence of veering or backing winds. A compelling, albeit anecdotal, piece of evidence comes from Fig. 11 of Rotunno and Klemp (1982), where the pressure gradient in a simulated storm aligns more with

the environmental shear than with the relative motion between storm and environment.

What we will see in section 2 is that the zero-drag and GKI schemes are equivalent, in the sense that the GKI scheme, with its tunable parameter C, predicts a CMT that is equal to $1 - C$ times that predicted by the ZD scheme. In other words,

$$\partial_t v|_{\mathrm{GKI}} = (1 - C)\partial_t v|_{\mathrm{ZD}}.$$

Section 3 will introduce the concept of a "transilient matrix for momentum." This matrix will be diagnosed from cloud-resolving simulations and will show that the GKI scheme underestimates the compensating subsidence of momentum by a factor of $1 - C$. Section 4 will demonstrate this same result from a high-resolution large-eddy simulation (LES). Finally, the results will be summarized in section 5.

2. Equivalence of ZD and GKI schemes

Let us approximate the atmosphere by two parts: cloud and environment. Using the standard bulk-plume model, we assume that vertical velocity and horizontal velocity are uncorrelated within each of those two classes. The continuity equations for cloud and environment are then

$$\partial_t(\sigma_c \rho) + \partial_z(\sigma_c \rho w_c) = e - d$$

$$\partial_t(\sigma_e \rho) + \partial_z(\sigma_e \rho w_e) = d - e$$

and the corresponding horizontal momentum equations are

$$\partial_t(\sigma_c \rho v_c) + \partial_z(\sigma_c \rho v_c w_c) = e v_e - d v_c + F$$

$$\partial_t(\sigma_e \rho v_e) + \partial_z(\sigma_e \rho v_e w_e) = d v_c - e v_e - F.$$

Here, $\sigma_c(z)$ is the fractional area of cloud and $\sigma_e = 1 - \sigma_c$ is the fractional area of environment. The entrainment and detrainment rates (kg m^{-3} s^{-1}) are denoted by e and d, respectively. The horizontal and vertical velocities are denoted by v and w with subscripts c and e to denote cloud and environment, respectively, and F is the horizontal force per volume between cloud and environment.

Assuming that clouds adjust much faster to a steady state than the environment does, we can drop the tendency terms in the cloud momentum equation and the two continuity equations. We also assume that $\sigma_c \ll 1$, so we can approximate σ_e by 1. For notational simplicity, we will now drop the e and c subscripts from all variables except v_c: from here on, σ and w are understood to be the cloud fractional area and cloud vertical velocity,

respectively, and v is the environment's horizontal wind speed. This simplifies the equations to

$$\partial_z M = e - d \tag{1}$$

$$\rho \partial_t v = \partial_z [M(v - v_c)] \tag{2}$$

$$\partial_z v_c = \varepsilon(v - v_c) + F/M, \tag{3}$$

where $M = \sigma \rho w$ is the convective mass flux and $\varepsilon = e/M$ is the fractional entrainment rate. Given the profiles of M and ε, the key to evaluating the tendency of the environmental wind is to calculate v_c from Eq. (3).

The zero-drag scheme is described by Eqs. (1)–(3) with F set to zero. We can integrate Eq. (3) with $F = 0$ to give

$$v_c(z) = v(z_0)e^{-\int_{z_0}^z dz' \varepsilon(z')}$$
$$+ \int_{z_0}^z dz' \varepsilon(z')v(z')e^{-\int_{z'}^z dz'' \varepsilon(z'')}, \tag{4}$$

where we have assumed that $v_c(z_0) = v(z_0)$. Using Eqs. (1) and (4) in Eq. (2), and defining the fractional detrainment rate $\delta = d/M$, we get

$$\rho \partial_t v(z) = M(z)\left[-\delta(z)v(z) + \partial_z v(z) \right.$$
$$+ \delta(z)v(z_0)e^{-\int_{z_0}^z dz' \varepsilon(z')}$$
$$\left. + \delta(z)\int_{z_0}^z dz' \varepsilon(z')v(z')e^{-\int_{z'}^z dz'' \varepsilon(z'')} \right]. \tag{5}$$

Note that v_c has been eliminated. This equation gives the tendency of $v(z)$ as a function of $v(z')$ for all $z' \in [z_0, z]$.

The GKI scheme is described by Eqs. (1)–(3) with $F = CM\partial_z v$, where C is a constant. Integrating Eq. (3) with $F = CM\partial_z v$ gives

$$v_c(z) = Cv(z) + (1 - C)v(z_0)e^{-\int_{z_0}^z dz' \varepsilon(z')}$$
$$+ (1 - C)\int_{z_0}^z dz' \varepsilon(z')v(z')e^{-\int_{z'}^z dz'' \varepsilon(z'')}, \tag{6}$$

where we have used the same boundary condition of $v_c(z_0) = v(z_0)$. Using Eqs. (1) and (6) in Eq. (2), we get

$$\rho \partial_t v(z) = (1 - C)M(z)\left[-\delta(z)v(z) + \partial_z v(z) \right.$$
$$+ \delta(z)v(z_0)e^{-\int_{z_0}^z dz' \varepsilon(z')}$$
$$\left. + \delta(z)\int_{z_0}^z dz' \varepsilon(z')v(z')e^{-\int_{z'}^z dz'' \varepsilon(z'')} \right]. \tag{7}$$

This is exactly the same as the ZD solution in Eq. (5), except that the right-hand side is multiplied by $1 - C$.

Therefore, for a given mass flux and entrainment rate, the wind tendency predicted by the GKI scheme is identical to $1 - C$ times the wind tendency predicted by the ZD scheme.

Since these two schemes differ by $1 - C$, we should be able to identify which is more accurate by comparing against cloud-resolving and large-eddy simulations. We can accomplish this by applying a horizontal force to a convecting atmosphere and then evaluating how convection redistributes that horizontal momentum. In particular, we will want to focus on the effect of compensating subsidence, which is represented by the $\partial_z v$ terms in Eqs. (5) and (7). There are several reasons for focusing on this term. For one, this term often plays a dominant role in convective momentum transport (Mapes and Wu 2001). Therefore, modeling this term correctly in a CMT scheme is of paramount importance. In addition, the effect of this term is relatively easy to measure and interpret: unlike the other terms in Eqs. (5) and (7), which involve ε and δ, the subsidence term involves only $\partial_z v$ and M, both of which are easy to calculate in a numerical simulation. Although ε and δ can be measured directly using the methods of Romps (2010) and Dawe and Austin (2011), it is not obvious how to relate these directly measured rates to the effective rates appropriate for a bulk-plume model such as Eqs. (1)–(3): Romps (2010) and Dawe and Austin (2011) showed that the directly measured values can differ significantly from the effective rates for the bulk-plume equations. Furthermore, the pressure force can alias onto ε and δ. For small $v - v_c$, a pressure force F that is a function of $v - v_c$ can be Taylor expanded to give $F = \beta M(v - v_c)$, for some $\beta(z)$. In this case, Eqs. (5) and (7) get modified by replacement of ε and δ with $\varepsilon + \beta$ and $\delta + \beta$, respectively. Note that the subsidence term is the one term whose interpretation is not complicated by the pressure force. Therefore, when $v - v_c$ is small, in the sense that F can be linearized, a DL scheme generates the same compensating subsidence as the ZD scheme. In summary, we will focus on the subsidence term because it is of great dynamical significance, its coefficient is straightforward to measure, and it is straightforward to interpret.

From Eq. (5), we see that the $\partial_z v$ term in the ZD scheme (and general DL schemes with small $v - v_c$) causes the wind profile to sink at a speed of M/ρ. From Eq. (7), we see that the GKI scheme causes the wind profile to sink at a speed of $(1 - C)M/\rho$. Our goal, then, is to diagnose the actual speed of momentum subsidence in cloud-resolving simulations to compare against these two predictions. Naively, we might consider initializing a cloud-resolving simulation with some wind profile and then watching as the wind profile descends with time. Unfortunately, there are effects in addition to compensating subsidence—that

is, the other terms in Eqs. (5) and (7)—that make the evolution of the wind profile more complicated than pure subsidence. To isolate the effect of the $\partial_z v$ term in cloud-resolving simulations, we will diagnose the transilient matrix (TM) for momentum.

3. Transilient matrix

Let us first define what we mean by a TM for momentum. The concept of a TM for mass was first introduced by Stull (1984), and it was shown by Romps and Kuang (2011) how to diagnose this matrix for moist convection. In general, a transilient matrix is the discretization of a transilient function (TF), which provides a linear map from the horizontally averaged profile of some quantity to the tendency of that profile due to convection. For example, the TF for horizontal momentum $b(z, z')$ is implicitly defined as

$$\rho \partial_t v(z)|_{\text{due to convection}} = \int dz' b(z, z') v(z'),$$

where v is the horizontally averaged wind in a particular direction. Similarly, the TM for horizontal momentum b_{ij} is implicitly defined as

$$\rho_i \partial_t v_i|_{\text{due to convection}} = \sum_j \Delta z_j b_{ij} v_j,$$

where i and j index vertical levels.

Note that Eqs. (5) and (7) can be written in terms of a transilient function. For the ZD scheme, $b(z, z')$ is given by

$$b(z, z') = -d(z)\delta_D(z' - z) - M(z)\partial_{z'}\delta_D(z' - z)$$
$$+ d(z)e^{-\int_{z_0}^{z} dz'' \varepsilon(z'')}\delta_D(z' - z_0)$$
$$+ d(z)\varepsilon(z')e^{-\int_{z'}^{z} dz'' \varepsilon(z'')}\mathcal{H}(z' - z_0)\mathcal{H}(z - z'), \quad (8)$$

where δ_D is the Dirac delta function and $\mathcal{H}$ is the Heaviside step function. For a given z, $b(z, z')$ is a sum of local distributions containing $\delta_D(z' - z)$, which gathers information on v only in the immediate vicinity of z (first two terms); $\delta_D(z' - z_0)$, which deposits momentum from z_0 (third term); and a nonlocal distribution that samples v at all $z' \in [z_0, z]$ (fourth term). The GKI scheme can be written in terms of a transilient function that is identical to Eq. (8) except for an overall coefficient of $1 - C$. For DL schemes with small $v - v_c$, the transilient function is given by Eq. (8) with the entrainment and detrainment rates modified by the addition of the linearized pressure force coefficients. For a discrete vertical grid, $b(z, z')$ becomes a matrix b_{ij}, whose indices range over the

vertical levels. By generalizing the method of Romps and Kuang (2011), we can diagnose this matrix directly from cloud-resolving simulations.

In Romps and Kuang (2011), it was possible to diagnose the TM for mass in a single simulation by injecting a unique radioactive tracer into each of the N vertical levels. Each tracer was advected passively with the flow with a steady source at its injection level and radioactive decay everywhere; the resulting distribution of tracers was used to infer b_{ij}. Note, however, that the TM for momentum is not, in general, the same as the TM for mass. This is because momentum can be transmitted between two parcels without exchanging any mass. Therefore, to diagnose a TM for momentum, it is not possible to use artificial tracers. Instead, we must use momentum as its own tracer. In this approach, horizontal momentum is uniformly injected into a vertical level (i.e., the air in that level is accelerated) and the horizontally averaged momentum is damped to zero with a time scale of 12 h, which is long compared to the time scale for vertical transport in a cloud [see the discussion in Romps and Kuang (2011)].

Since there are only two independent components of momentum (x and y), we must run multiple simulations. In principle, $N/2$ simulations could be run, where N is the number of vertical levels. For simplicity, however, N simulations are run, each of which has x momentum injected into a corresponding level. The cloud-resolving model used for these simulations is Das Atmosphärische Modell (DAM; Romps 2008). The simulations use the same doubly periodic domain (32 km $\times$ 32 km $\times$ 30 km), grid spacings (2-km horizontal, variable vertical), radiation (equator, 1 January, no diurnal cycle), and lower boundary (300-K ocean) as used by Romps and Kuang (2011), which gives deep marine convection in radiative–convective equilibrium (RCE). To simplify the analysis of the momentum budget, the lower boundary is specified to be free slip. To avoid feedbacks on the surface fluxes, a bulk aerodynamic formula is used with a fixed wind speed of 5 m s^{-1}.

The transilient matrix is a linear operator, which implies that the quantity being transported by convection does not affect the convection itself. For horizontal momentum, this is not necessarily the case: a sufficiently large shear can blow apart convecting clouds, altering the convective mass fluxes. Therefore, we wish to use an applied force that is small enough to ensure the passivity of momentum transport. However, we also want a good signal-to-noise ratio in the resulting wind profile, which is obtained with a stronger applied force. This trade-off is explored using nine different sets of simulations, each with a different magnitude of forcing applied to a single vertical level. The applied forcing ranges from 3.125×10^{-5} to

8×10^{-3} m s^{-2} by factors of 2. Since there are 64 vertical levels in the cloud-resolving simulation, this requires $64 \times 9 = 576$ cloud-resolving simulations, each of which is run for 60 days with the first 2 days discarded as spinup. Figure 1 shows the peak value of the steady-state wind profile v normalized by the applied forcing A, plotted as a function of applied forcing. There are 64 curves, each corresponding to the forcing being applied to a particular level. If the response were linear, as desired, then the curves would all be flat at a normalized value of one. Up to an applied forcing of about 5×10^{-4} m s^{-2}, the response remains linear for most levels, so this is the acceleration used in the calculation of the transilient matrix. The three levels with the largest deviations from linearity are the lowest three layers, which suggest that the transilient matrix may not be as reliable in the vicinity of the surface.

Now, let $S(z)$ be a constant external source of horizontal momentum and let τ be the time scale over which momentum is damped to zero. Then, the mean wind profile $v(z, t)$ evolves as

$$\partial_t[\rho(z)v(z,t)] = S(z) - \rho(z)v(z,t)/\tau + \int dz'\, b(z,z')v(z',t),$$

where the three terms on the right-hand side correspond to the external forcing, Rayleigh damping, and convective momentum transport, respectively. Following Romps and Kuang (2011), we can discretize this equation into N height levels (corresponding to the N levels of the cloud-resolving simulation). By diagnosing the wind profile from N different simulations (each with a different and linearly independent profile S), we can assemble the N equations for v into a matrix equation that can be solved for b_{ij}. Analogous to Eq. (9) in Romps and Kuang (2011), the transilient matrix for momentum is diagnosed as

$$b_{ij} = \frac{1}{\Delta z_j} \sum_k \left[\partial_t(\rho_i v_{ik}) + \frac{\rho_i v_{ik}}{\tau} - S_{ik} \right] (v^{-1})_{kj}, \quad (9)$$

where v_{ik} is the horizontally averaged x velocity at height i in simulation k, S_{ik} is the applied acceleration at height i in simulation k ($S_{ik} = a\delta_{ik}$, where $a/\rho_i = 5 \times 10^{-4}$ m s^{-2}), ρ_i is the air density at height i, Δz_j is the vertical grid spacing at height j (ranging from 50 m near the surface to 500 m in the midtroposphere to 1000 m in the stratosphere), and τ is the damping time of 12 h. Each simulation was run for 2 months with the v_{ik} and $\partial_t v_{ik}$ averaged over all but the first 2 days, which were discarded as spinup. Putting the resulting v_{ik} and $\partial_t v_{ik}$ into Eq. (9) gives the result shown in Fig. 2. The left panel displays the matrix in units of kg m^{-4} s^{-1}. Hewing to convention, the matrix is displayed upside down so
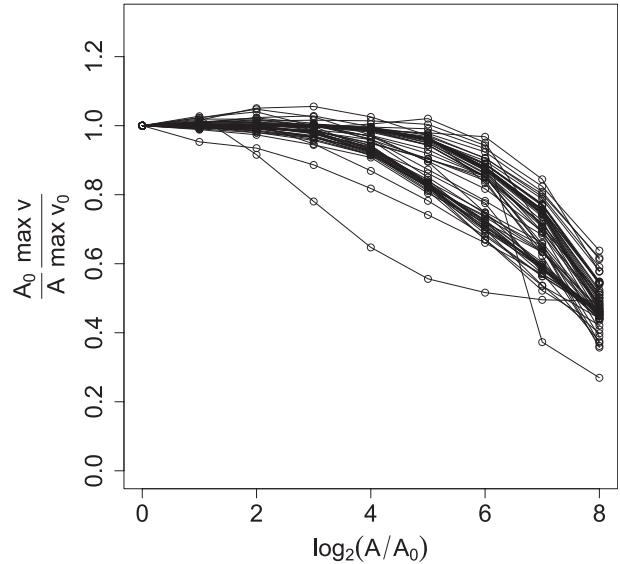
FIG. 1. Ratio of the maximum value of v divided by the applied forcing A, and normalized by the value of this ratio for the smallest forcing (an acceleration of 3.125×10^{-5} m s^{-2}). Each curve corresponds to a set of cloud-resolving RCE simulations in which the forcing is applied to a particular vertical level.

that the destination height (on the y axis) increases upward. The right panel plots a sample row of the matrix.

As we see from Fig. 2, the most prominent matrix elements are in the vicinity of the diagonal. These elements constitute the local operators, which are larger than other elements of the matrix because they contain factors of $1/\Delta z$. For example, $\int dz'\, b(z,z')f(z')$ acts as the unit operator on f when the transilient function $b(z, z')$ is a delta function, which corresponds to a transilient matrix with $1/\Delta z$ on the diagonal. Other local operators—such as ∂_z and ∂_z^2—are represented in b_{ij} by the finite-difference approximations to those derivatives. The order of accuracy of these stencils will depend on the highest-order local operator that is contained in the matrix. Table 1 gives examples of the mappings between operators, transilient functions, and transilient matrices for the case of a constant vertical grid spacing and with local operators confined to a three-point stencil (i.e., in which the highest-order operator is ∂_z^2).

It is clear from the second panel of Fig. 2 that the local operators occupy a five-point stencil. For each row of b_{ij}, the five elements $\{b_{i,i-2}, \ldots, b_{i,i+2}\}$ form a stencil that can be decomposed into operators proportional to 1, ∂_z, ∂_z^2, ∂_z^3, and ∂_z^4 (see appendix A). We write the coefficients of these operators as c_0 through c_4. These coefficients will, in general, be a function of height. For our purposes, we are interested in $c_1(z)$ because this is the coefficient of ∂_z, the operator corresponding to subsidence. The drag-law scheme predicts that the wind profile
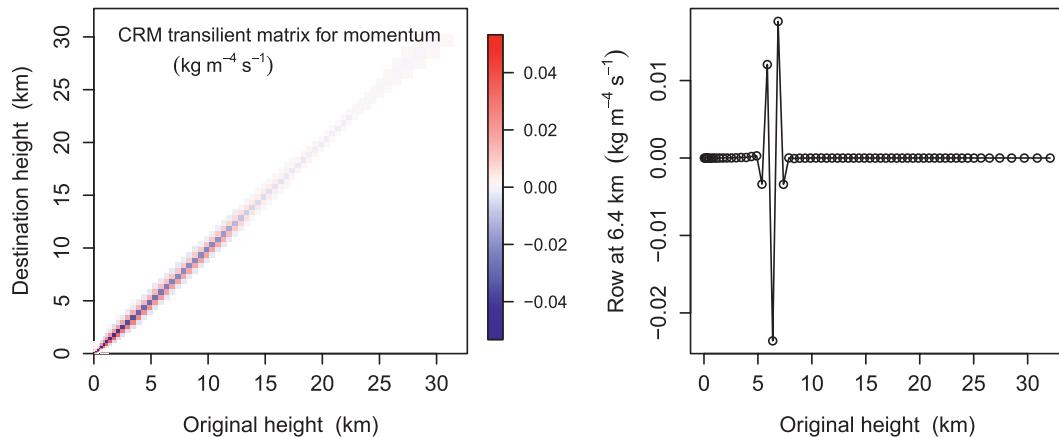
FIG. 2. (left) TM for momentum diagnosed from the cloud-resolving model (kg m^{-4} s^{-1}). (right) A row of the matrix for a destination height of 6.4 km.

subsides at a speed of $c_1/\rho = M/\rho$, and the Gregory–Kershaw–Inness scheme predicts $c_1/\rho = (1 - C)M/\rho$.

Figure 3 plots the value of c_1/ρ diagnosed from the transilient matrix (solid line). This is the speed at which momentum subsides in the cloud-resolving simulations. The dashed line plots the speed M/ρ at which mass subsides, which is also the DL prediction for the speed of momentum subsidence. Here, the convective mass flux M is diagnosed as the horizontally and temporally averaged value of $\mathcal{A}\rho w$, where $\mathcal{A}$ is unity where $w \geq 1$ m s^{-1} and the condensed-water mixing ratio q_c satisfies $q_c \geq 10^{-5}$ kg kg^{-1}, and is zero elsewhere (e.g., Romps and Kuang 2010). Overall, we see that the DL prediction is an excellent match with the diagnosed subsidence. The main differences are found in and above the tropical tropopause layer (TTL) and in the subcloud layer. In the TTL and above, the transilient matrix reports a small downward subsidence of momentum, presumably due to the action of gravity waves. Below the cloud base, which is located at 500 m, the DL prediction is zero because there is no cloud mass flux. Dry eddies are likely responsible for the momentum subsidence seen there. In the cloud layer, we can conclude that momentum subsides at the same speed as mass. The GKI prediction for

the speed of momentum subsidence (dotted line) is too small by a factor of $1 - C$.

4. Large-eddy simulation

We can also confirm this result in a large-eddy simulation. Unfortunately, LES is too computationally expensive to allow for constructing a transilient matrix, which requires as many simulations as there are vertical levels. Instead, we can examine the response to an applied

TABLE 1. The correspondence between local operators, the TF, and the TM in the case of a constant vertical spacing Δ and with operators confined to a tridiagonal.

Operator	$b(z, z')$	$(\ldots,$	$b_{i,i-1}$	$, b_{i,i}$	$, b_{i,i+1}$	$, \ldots)$
1	$\delta_D(z - z')$	$\ldots,$	0	$, \frac{1}{\Delta}$	$, 0$	$, \ldots$
∂_z	$-\partial_{z'}\delta_D(z - z')$	$\ldots,$	$-\frac{1}{2\Delta^2}$	$, 0$	$, \frac{1}{2\Delta^2}$	$, \ldots$
∂_z^2	$\partial_{z'}^2\delta_D(z - z')$	$\ldots,$	$\frac{1}{\Delta^3}$	$, -\frac{2}{\Delta^3}$	$, \frac{1}{\Delta^3}$	$, \ldots$
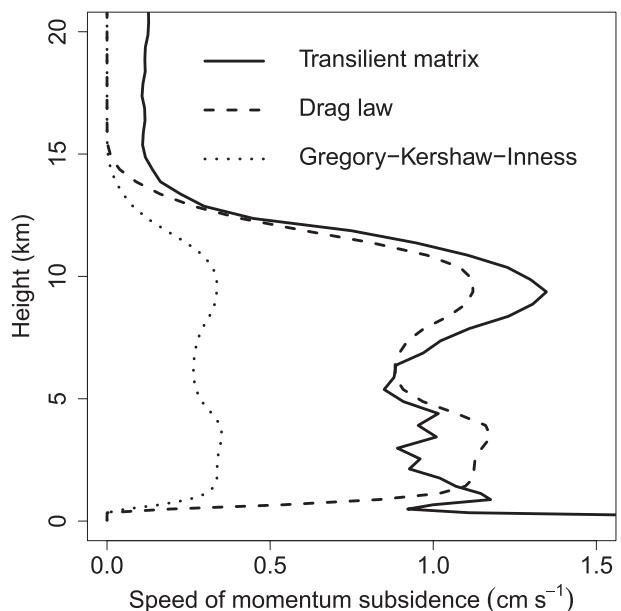
FIG. 3. Speed at which the wind profile subsides (c_1/ρ) as measured by the TM diagnosed from cloud-resolving simulations (solid). Also shown are the DL prediction of M/ρ for the subsidence speed (dashed), and the GKI prediction of $(1 - C) M/\rho$ with $C = 0.7$ (dotted).

forcing in a single simulation and compare the resulting winds to the predictions from the CMT schemes.

The LES used here has a horizontal grid spacing of 200 m and a vertical spacing of 50 m between 3 and 15 km. The doubly periodic horizontal domain is 38.4 km $\times$ 38.4 km, and the model top is at 30 km. An acceleration of $a = 5 \times 10^{-4}$ m s^{-2} (the same as in the previous section) is applied on a single grid level at 6 km, which corresponds to an applied external force of $A = a\rho\Delta z = 0.016$ N m^{-2}. As in the previous section, the horizontally averaged momentum is damped to zero on a time scale of $\tau = 12$ h. The simulation is run to equilibrium for over a week, and statistics are collected over the last 3 days.

Qualitatively, what sort of steady-state wind profile should we expect from this simulation? Applying an external force A (N m^{-2}) at injection height z_i, damping the wind to zero over a time scale τ, and assuming a steady state, Eqs. (2) and (3) become

$$0 = \partial_z[M(v - v_c)] + A\delta_D - \rho v/\tau \qquad (10)$$

$$\partial_z v_c = \varepsilon(v - v_c) + F/M, \qquad (11)$$

where $\delta_D = \delta_D(z - z_i)$ is centered on z_i. For the moment, let us assume that $F = 0$. As shown in appendix B, the full analytical solution to these equations for zero F and constant M, ε, and ρ is

$$v = \frac{\varepsilon + \lambda_{\text{sign}(z_i-z)}}{\lambda_+ - \lambda_-} \frac{A}{M} \exp[\lambda_{\text{sign}(z_i-z)}(z - z_i)], \qquad (12)$$

$$v_c = \frac{\varepsilon}{\lambda_+ - \lambda_-} \frac{A}{M} \exp[\lambda_{\text{sign}(z_i-z)}(z - z_i)], \qquad (13)$$

where

$$\lambda_\pm = \frac{\rho}{2M\tau}\left(1 \pm \sqrt{1 + 4M\varepsilon\tau/\rho}\right). \qquad (14)$$

Equation (12) for v takes the form of two exponentials stitched together discontinuously at z_i. Equation (13) for v_c takes the form of two exponentials stitched together continuously at z_i.

In this solution, the ratio of the wind speed v just above z_i to the wind speed just below z_i is equal to

$$\frac{2x + 1 - \sqrt{1 + 4x}}{2x + 1 + \sqrt{1 + 4x}}, \qquad (15)$$

where $x = M\varepsilon\tau/\rho$. This ratio is plotted in Fig. 4. For tropical RCE, typical midtropospheric values are $M = 0.01$ kg m^{-2} s^{-1}, $\rho = 0.5$ kg m^{-3}, and $\varepsilon \lesssim 1$ km^{-1}. For $\tau = 12$ h as used here, $M\varepsilon\tau/\rho \lesssim 1$. According to Fig. 4, this means that the wind speed just above z_i is $\lesssim 10\%$ the
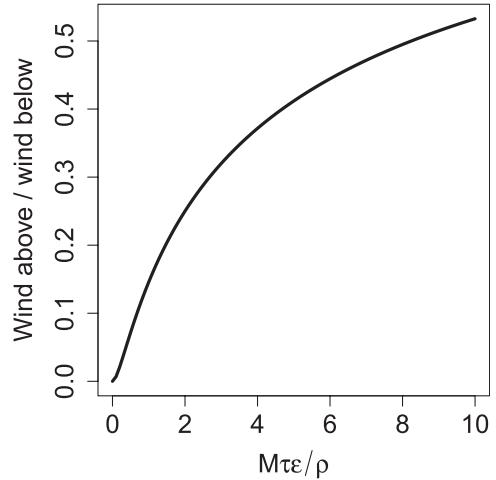
FIG. 4. Equation (15) plotted as a function of $M\tau\varepsilon/\rho$, which gives, for the full analytical solution in Eq. (12), the ratio of the wind speed just above the applied acceleration to the wind speed just below.

wind speed just below z_i. Therefore, we can approximate the solution for v to within an error of 10% by setting ε to zero. This gives

$$v = \frac{A}{M} \exp\left[\frac{\rho}{M\tau}(z - z_i)\right]\mathcal{H}(z_i - z), \qquad (16)$$

$$v_c = 0. \qquad (17)$$

In this approximation, convection acts only to advect the wind profile downward with the speed M/ρ.

A similar conclusion applies to the case where the pressure force on the cloud is described by some function $F(v - v_c)$. For sufficiently small $v - v_c$, we can Taylor expand F. Noting that $F(0) = 0$ by symmetry, the Taylor expansion to first order gives $F = F'(0)(v - v_c)$. Adding this pressure force simply modifies Eqs. (12) and (13) by replacement of ε with $\varepsilon + F'(0)/M$. Therefore, Eq. (16) is a good approximation so long as $[M\varepsilon + F'(0)]\tau/\rho \lesssim 1$. Figure 5 shows the full analytical solution [Eqs. (12) and (13)] and the simplified analytical solution [Eqs. (16) and (17)] for the values of M, ρ, and ε diagnosed at 6 km in the LES. For the full analytical solution, the value of ε is calculated using the direct measurement technique of Romps (2010). As expected, the full and simplified analytical expressions for v are in close agreement. This is the shape of the wind profile v that we should expect to see in both the LES and a faithful CMT scheme.

The average wind profile v from the LES is shown in Fig. 6 as the solid line. As in Fig. 5, the simplified analytical expression is plotted as the dashed line. We see that the simplified analytical expression does an excellent job of predicting the shape of the LES wind profile v. Since the shape and magnitude of the analytical profile is set by the
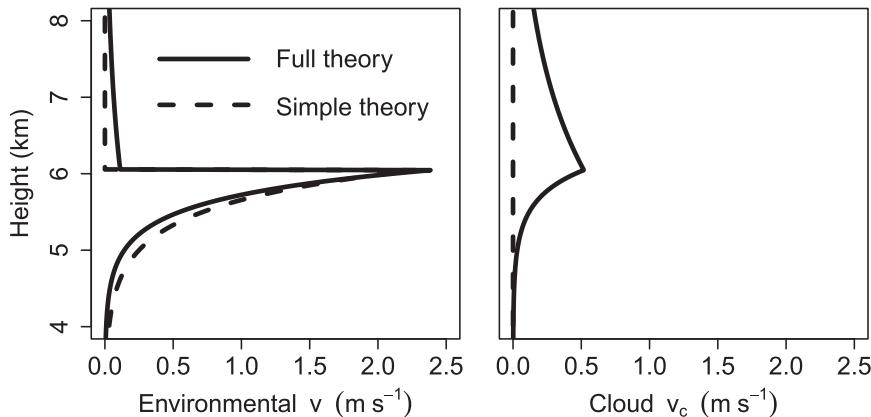
FIG. 5. (left) Environmental wind speed and (right) cloud wind speed for the full analytic solution in Eqs. (12) and (13) (solid), and the simplified analytic solution in Eqs. (16) and (17) (dashed).

subsidence rate M, this confirms that momentum subsides at a speed equal to M/ρ. In addition, the similarity between the LES v in Fig. 6 and the full analytic v in Fig. 5 is striking.

In contrast, the simplified v profile predicted by the GKI scheme is given by Eq. (16) with M replaced by $(1 - C)M$. This prediction is shown in Fig. 6 as a dotted line. This confirms the conclusion from section 3: parameterizing the pressure gradient force as $F = CM\partial_z v$, as in the GKI scheme, causes the wind profile to subside too slowly by a factor of $1 - C$.

5. Summary and discussion

We have seen that the Gregory–Kershaw–Inness (GKI) scheme for convective momentum transport (Gregory et al. 1997), which is the default in CAM5.1, is exactly proportional to the zero-drag (ZD) scheme, which has no parameterization of the pressure force. That constant of proportionality is $1 - C$, where C is specified to be 0.7 by GKI and Richter and Rasch (2008), and 0.55 by Zhang and Wu (2003). In CAM5.1, C is set to 0.4. The findings presented here suggests that C should be set all the way to zero, which would make the GKI

scheme identical to the ZD scheme. This fits well with the results of Richter and Rasch (2008), who found that the ZD scheme (which they refer to as SL76) produced a more realistic climate than the GKI scheme (which they refer to as GKI97). Setting C to zero also eliminates a potential numerical instability in the GKI scheme (Kershaw et al. 2000).

APPENDIX A

Operator Decomposition

Given the discretization $q_i = q(z_i)$ for $i = 1, \ldots, N$ of some profile $q(z)$, the derivatives up to fourth order of $q(z)$ at z_i can be approximated by

$$
\begin{pmatrix} q(z_i) \\ \partial_z q(z_i) \\ \vdots \\ \partial_z^4 q(z_i) \end{pmatrix} \approx \mathsf{S} \begin{pmatrix} q_{i-2} \\ q_{i-1} \\ \vdots \\ q_{i+2} \end{pmatrix},
$$

where S is a stencil matrix. Since S is a nondegenerate matrix, there exist coefficients $c_{ip} = c_p(z_i)$ such that
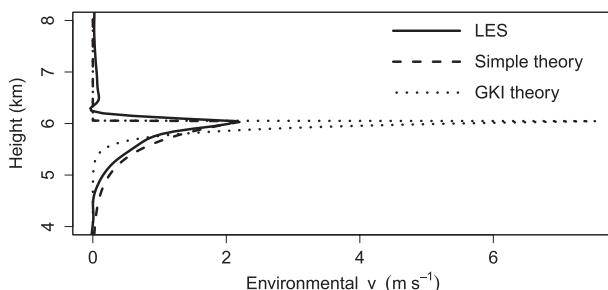
FIG. 6. Environmental wind speed as diagnosed in the LES (solid), as predicted by the simple theory of Eq. (16) (dashed), and as predicted by the GKI scheme (dotted), which is Eq. (16) with M replaced by $(1 - C)M$ for $C = 0.7$.

$$\int dz\, b(z_i, z)q(z) \approx \sum_j \Delta z_j b_{ij} q_j = \sum_{p=1}^{5} \Delta z_{i+p-3} b_{i,i+p-3} q_{i+p-3} + \text{NLT} = \sum_{r,p=1}^{5} c_{i,r-1} S_{rp} q_{i+p-3} + \text{NLT}$$

$$\approx \sum_{r=1}^{5} c_{r-1}(z_i) \partial_z^{r-1} q(z_i) + \text{NLT},$$

where

$$\text{NLT} = \sum_{j \notin [i-2, i+2]} \Delta z_j b_{ij} q_j$$

are the nonlocal terms. We see that the near-diagonal elements of **b** can be expressed in terms of the coefficients $(c_0, c_1, \ldots, c_4)$ of local operators $(1, \partial_z, \ldots, \partial_z^4)$, where the coefficient c_p has units of kg m^{p-3} s^{-1}. These coefficients are related to the transilient matrix via

$$c_{r-1}(z_i) = \sum_{p=1}^{5} b_{i,i+p-3} \Delta z_{i+p-3} T_{pr},$$

where $\mathbf{T} \equiv \mathbf{S}^{-1}$ is the matrix of Taylor series coefficients.

APPENDIX B

Analytical Wind Profile

Consider Eqs. (10) and (11) with M, ε, ρ, and τ that are constant with height and $F = 0$. Assuming that $v_c(z_0) = v(z_0)$ for some z_0, we can integrate Eq. (11) to give

$$v_c(z) = \varepsilon e^{-\varepsilon z} \int_{z_0}^{z} dz'\, e^{\varepsilon z'} v(z') + e^{-\varepsilon(z-z_0)} v(z_0). \quad \text{(B1)}$$

Plugging this into Eq. (10) gives

$$M\partial_z v(z) + M\varepsilon^2 e^{-\varepsilon z} \int_{z_0}^{z} dz'\, e^{\varepsilon z'} v(z') - M\varepsilon v(z)$$

$$+ M\varepsilon e^{-\varepsilon(z-z_0)} v(z_0) - \rho(z)v(z)/\tau + A\delta_D = 0. \quad \text{(B2)}$$

When $A = 0$, we can look for solutions of the form $v = e^{\lambda z}$. For $v(z_0) = 0$ and z far from z_0, in the sense that $(z - z_0)\rho/M\tau \gg 1$, $v = e^{\lambda_+ z}$, and $v = e^{\lambda_- z}$ are solutions when $A = 0$ and

$$\lambda_\pm = \frac{\rho}{2M\tau}\left(1 \pm \sqrt{1 + 4M\varepsilon\tau/\rho}\right).$$

For $A \neq 0$, the solution can be found by stitching together these two exponential solutions to either side of z_i. To satisfy the requirement that $v = 0$ at $z = \pm\infty$, we need to use λ_+ for $z < z_i$ and λ_- for $z > z_i$. Let us denote the amplitude of v just below and above z_i by C_1 and C_2, respectively. Integrating Eq. (B2) over an infinitesimal height interval centered on z_i reveals that $C_1 = C_2 + A/M$. When we integrate Eq. (B2) over all heights (again, neglecting terms involving an exponential of z_0), we find that the sum of the first four terms integrate to zero identically. This is a consequence of the fact that those terms represent the rearrangement of momentum in the vertical: they cannot generate a net source or sink of momentum. Therefore, the integral of Eq. (B2) over all z reduces to

$$0 = \int_{z_0}^{\infty} dz\left(-\frac{\rho v}{\tau} + A\delta_D\right) = A - \frac{\rho}{\tau}\left(\frac{C_1}{\lambda_+} - \frac{C_2}{\lambda_-}\right).$$

Using $C_1 = C_2 + A/M$ reveals the solution given in Eq. (12). Substituting this expression into Eq. (B1) gives Eq. (13).

REFERENCES

Austin, P. M., and R. A. Houze, 1973: A technique for computing vertical transports by precipitating cumuli. *J. Atmos. Sci.,* **30,** 1100–1111.

Dawe, J. T., and P. H. Austin, 2011: The influence of the cloud shell on tracer budget measurements of LES cloud entrainment. *J. Atmos. Sci.,* **68,** 2909–2920.

Gregory, D., R. Kershaw, and P. M. Inness, 1997: Parametrization of momentum transport by convection. II: Tests in single-column and general circulation models. *Quart. J. Roy. Meteor. Soc.,* **123,** 1153–1183, doi:10.1002/qj.49712354103.

Hitschfeld, W., 1960: The motion and erosion of convective storms in severe vertical wind shear. *J. Atmos. Sci.,* **17,** 270–282.

Houze, R. A., 1973: A climatological study of vertical transports by cumulus-scale convection. *J. Atmos. Sci.,* **30,** 1112–1123.

Jorgensen, D. P., M. A. LeMone, and B. Jong-Dao Jou, 1991: Precipitation and kinematic structure of an oceanic mesoscale convective system. Part I: Convective line structure. *Mon. Wea. Rev.,* **119,** 2608–2637.

Kershaw, R., A. L. M. Grant, S. H. Derbyshire, and S. Cusack, 2000: The numerical stability of a parametrization of convective momentum transport. *Quart. J. Roy. Meteor. Soc.,* **126,** 2981–2984.

Kim, D., J.-S. Kug, I.-S. Kang, F.-F. Jin, and A. T. Wittenberg, 2008: Tropical Pacific impacts of convective momentum transport in the SNU coupled GCM. *Climate Dyn.,* **31,** 213–226.

Lafore, J. P., J. L. Redelsperger, and G. Jaubert, 1988: Comparison between a three-dimensional simulation and Doppler radar data of a tropical squall line: Transport of mass, momentum, heat, and moisture. *J. Atmos. Sci.,* **45,** 3483–3500.

Lane, T. P., and M. W. Moncrieff, 2010: Characterization of momentum transport associated with organized moist convection and gravity waves. *J. Atmos. Sci.,* **67,** 3208–3225.

LeMone, M. A., 1983: Momentum transport by a line of cumulonimbus. *J. Atmos. Sci.,* **40,** 1815–1834.

——, G. M. Barnes, and E. J. Zipser, 1984: Momentum flux by lines of cumulonimbus over the tropical oceans. *J. Atmos. Sci.,* **41,** 1914–1932.

——, ——, J. C. Fankhauser, and L. F. Tarleton, 1988: Perturbation pressure fields measured by aircraft around the cloud-base updraft of deep convective clouds. *Mon. Wea. Rev.,* **116,** 313–327.

Lin, Y. J., T. C. Wang, and J. H. Lin, 1986: Pressure and temperature perturbations within a squall-line thunderstorm derived from SESAME dual-Doppler data. *J. Atmos. Sci.,* **43,** 2302–2327.

Malkus, J. S., 1952: The slopes of cumulus clouds in relation to external wind shear. *Quart. J. Roy. Meteor. Soc.,* **78,** 530–542.

Mapes, B. E., and X. Wu, 2001: Convective eddy momentum tendencies in long cloud-resolving model simulations. *J. Atmos. Sci.,* **58,** 517–526.

Moncrieff, M. W., 1992: Organized convective systems: Archetypal dynamical models, mass and momentum flux theory, and parametrization. *Quart. J. Roy. Meteor. Soc.,* **118,** 819–850.

——, and M. J. Miller, 1976: The dynamics and simulation of tropical cumulonimbus and squall lines. *Quart. J. Roy. Meteor. Soc.,* **102,** 373–394.

Neale, R. B., J. H. Richter, and M. Jochum, 2008: The impact of convection on ENSO: From a delayed oscillator to a series of events. *J. Climate,* **21,** 5904–5924.

——, and Coauthors, 2010: Description of the NCAR Community Atmosphere Model (CAM 5.1). NCAR Tech. Note NCAR/TN-486+STR, 286 pp.

Newton, C. W., 1966: Circulations in large sheared cumulonimbus. *Tellus,* **18,** 699–713.

——, and H. R. Newton, 1959: Dynamical interactions between large convective clouds and environment with vertical shear. *J. Atmos. Sci.,* **16,** 483–496.

Ramond, D., 1978: Pressure perturbations in deep convection: An experimental study. *J. Atmos. Sci.,* **35,** 1704–1711.

Richter, J. H., and P. J. Rasch, 2008: Effects of convective momentum transport on the atmospheric circulation in the Community Atmosphere Model, version 3. *J. Climate,* **21,** 1487–1499.

Robe, F. R., and K. A. Emanuel, 2001: The effect of vertical wind shear on radiative–convective equilibrium states. *J. Atmos. Sci.,* **58,** 1427–1445.

Romps, D. M., 2008: The dry-entropy budget of a moist atmosphere. *J. Atmos. Sci.,* **65,** 3779–3799.

——, 2010: A direct measure of entrainment. *J. Atmos. Sci.,* **67,** 1908–1927.

——, and Z. Kuang, 2010: Do undiluted convective plumes exist in the upper tropical troposphere? *J. Atmos. Sci.,* **67,** 468–484.

——, and ——, 2011: A transilient matrix for moist convection. *J. Atmos. Sci.,* **68,** 2009–2025.

Rotunno, R., and J. B. Klemp, 1982: The influence of the shear-induced pressure gradient on thunderstorm motion. *Mon. Wea. Rev.,* **110,** 136–151.

Sanders, F., and K. A. Emanuel, 1977: The momentum budget and temporal evolution of a mesoscale convective system. *J. Atmos. Sci.,* **34,** 322–330.

Schneider, E. K., and R. S. Lindzen, 1976: A discussion of the parameterization of momentum exchange by cumulus convection. *J. Geophys. Res.,* **81** (18), 3158–3160.

Shapiro, L. J., and D. E. Stevens, 1980: Parameterization of convective effects on the momentum and vorticity budgets of synoptic-scale Atlantic tropical waves. *Mon. Wea. Rev.,* **108,** 1816–1826

Soong, S. T., and W. K. Tao, 1984: A numerical study of the vertical transport of momentum in a tropical rainband. *J. Atmos. Sci.,* **41,** 1049–1061.

Stull, R. B., 1984: Transilient turbulence theory. Part I: The concept of eddy-mixing across finite distances. *J. Atmos. Sci.,* **41,** 3351–3367.

Sui, C.-H., M.-D. Cheng, X. Wu, and M. Yanai, 1989: Cumulus ensemble effects on the large-scale vorticity and momentum fields of GATE. Part II: Parametrization. *J. Atmos. Sci.,* **46,** 1609–1629.

Tao, W.-K., and S.-T. Soong, 1986: A study of the response of deep tropical clouds to mesoscale processes: Three-dimensional numerical experiments. *J. Atmos. Sci.,* **43,** 2653–2676.

Wu, X., and M. Yanai, 1994: Effects of vertical wind shear on the cumulus transport of momentum: Observations and parameterization. *J. Atmos. Sci.,* **51,** 1640–1660.

——, L. Deng, X. Song, and G. J. Zhang, 2007: Coupling of convective momentum transport with convective heating in global climate simulations. *J. Atmos. Sci.,* **64,** 1334–1349.

Zhang, G. J., and H.-R. Cho, 1991: Parameterization of the vertical transport of momentum by cumulus clouds. Part I: Theory. *J. Atmos. Sci.,* **48,** 1483–1492.

——, and X. Wu, 2003: Convective momentum transport and perturbation pressure field from a cloud-resolving model simulation. *J. Atmos. Sci.,* **60,** 1120–1139.